Supporting Information for "Primary events in the blue light sensor plant cryptochrome: intraprotein electron and proton transfer revealed by femtosecond spectroscopy"

Dominik Immeln,[†] Alexander Weigel,[‡] Tilman Kottke,[*,†] and J. Luis Pérez Lustres[*,‡,¶]

Physical and Biophysical Chemistry, Department of Chemistry, Bielefeld University, Universitätsstr. 25, 33615 Bielefeld, Germany, Humboldt Universität zu Berlin, Institut für Chemie, Brook Taylor Str. 2, D-12489 Berlin, Germany, and Research Center for Biological Chemistry and Molecular Materials (CIQUS), Department of Physical Chemistry, University of Santiago, c/ Jenaro de la Fuente s/n, E-15782 Santiago, Spain

E-mail: tilman.kottke@uni-bielefeld.de; luis.lustres@usc.es

Anisotropy measurements in femtosecond broadband transient absorption

The femtosecond transient absorption anisotropy $r(t)$ is constructed from measurements done with parallel $\Delta A_{\parallel}(t)$ and perpendicular $\Delta A_{\perp}(t)$ pump-probe polarizations, according to the definition in

[*]To whom correspondence should be addressed
[†]Bielefeld University
[‡]Humboldt Universität zu Berlin
[¶]University of Santiago

Equation 1.

$$r(t) = \frac{\Delta A_{\parallel}(t) - \Delta A_{\perp}(t)}{\Delta A_{\parallel}(t) + 2\Delta A_{\perp}(t)} \tag{1}$$

The anisotropy contains information about the orientation of excited-state transition dipoles relative to that of the ground-state transition used for optical pumping. To understand its meaning, we first relate the transient absorption to the light intensity absorbed by the excited-state population. In the limit of small absorption, $\Delta A \approx I_a^*/I_t \propto \left[g_{1n}(\nu)\mu_{1n}^2 \left\langle \cos^2\theta_{1n}\right\rangle - g_{01}(\nu)\mu_{01}^2 \left\langle \cos^2\theta_{01}\right\rangle\right]$, where I_a^* is the intensity absorbed by the excited population, I_t the transmitted intensity before the pump pulse impinges the sample, $g_{ij}(\nu)$ is a lineshape function for the $i \rightarrow j$ optical transition and μ_{ij} is the strength of the associated transition dipole moment. θ_{ij} is the angle between the transition dipole moment of the optical transition and the polarization vector of the probe field and $\langle\rangle$ means an ensemble average. Therefore, the transient absorption signals entering 1 are proportional to the difference between the squared transition dipoles of ground- and excited-state populations weighted by their lineshape functions and orientational factors. The expression may be easily generalized for more than two overlapping transitions.

Next, *photoselection* by the pump field is taken into account. The electric dipole transition probability is proportional to the $\cos^2\theta_P$, where θ_P is the angle between the pump electric field polarization vector and the transition dipole moment ($\vec{\mu}_{01}$, for the $S_0 \rightarrow S_1$ optical transition). Thus, the interaction with the pump pulse generates a spherically-symmetric anisotropic distribution of transition dipoles (fixed in the molecular frame) around the polarization vector at early time. This phenomenon is known as *photoselection.* The distribution is then probed by the probe field which is polarized either parallel or perpendicular to the pump in our experiments. This gives rise to a polarization-dependent signal strength since absorption of probe light is again proportional to $\cos^2\theta_{Pr}$, where θ_{Pr} is the angle between the transition dipole ($\vec{\mu}_{1n}$, for a given $S_1 \rightarrow S_n$ optical transition) and the polarization vector of the probe field. The signal strength is evaluated by considering an isotropic orientational distribution before interaction with the pump pulse. The isotropic probability of finding a molecule between angles θ_P and $\theta_P + d\theta_P$ is proportional to

$\sin\theta_P d\theta_P$. The normalized probability distribution is then multiplied by the excitation probability $\cos^2\theta_P$, by the probe absorption probability $\cos^2\theta_{Pr}$ and integrated to full space. Therefore $\Delta A \propto g_{01}(\nu_P)g_{1n}(\nu_{Pr})\mu_{01}^2\mu_{1n}^2\frac{\int\cos^2\theta_{Pr}\cos^2\theta_P\sin\theta_P d\theta_P d\varphi}{\int\sin\theta_P d\theta_P d\varphi}$ for parallel $\vec{\mu}_{01}$ and $\vec{\mu}_{1n}$ transition dipoles and a single excited-state optical transition. Overlap with ground-state bleach is neglected in the subsequent discussion for the sake of conciseness.

The following cases are discussed next: a) parallel $\vec{\mu}_{01}$ and $\vec{\mu}_{1n}$ transition dipoles; b) non-parallel $\vec{\mu}_{01}$ and $\vec{\mu}_{1n}$ transition dipoles and c) overlapping excited-state absorption (ESA) and stimulated emission (SE) bands with non-parallel transition dipoles. We limit ourselves to the time-zero anisotropy, *i.e.* before rotational diffusion has started.

- **Case a, parallel $\vec{\mu}_{01}$ and $\vec{\mu}_{1n}$ transition dipoles.** If $\vec{\mu}_{01}$ and $\vec{\mu}_{1n}$ transition dipoles and the pump and probe fields are parallel, θ_P equals θ_{Pr} and the transient absorption signal is given by Equation 2.

$$\Delta A_{\parallel}^0 \propto g_{01}(\nu_P)g_{1n}(\nu_{Pr})\mu_{01}^2\mu_{1n}^2\frac{\int_0^\pi\cos^2\theta_P\cos^2\theta_P\sin\theta_P d\theta_P\int_0^{2\pi}d\varphi}{\int_0^\pi\sin\theta_P d\theta_P\int_0^{2\pi}d\varphi} \tag{2}$$

  By integrating the *rhs* we obtain that $\Delta A_{\parallel}^0 \propto \frac{1}{5}$. The cosine theorem of spherical trigonometry is used to calculate the signal for perpendicular pump-probe polarization. If ψ is defined as the dihedral angle between the plane containing the pump and probe polarization vectors and that containing the pump polarization vector and $\vec{\mu}_{01}$, the transient absorption signal obeys Equation 3.

$$\Delta A_{\perp}^0 \propto g_{01}(\nu_P)g_{1n}(\nu_{Pr})\mu_{01}^2\mu_{1n}^2\frac{\int_0^\pi\cos^2\theta_P\sin^2\theta_P\sin\theta_P d\theta_P\int_0^{2\pi}d\varphi\int_0^{2\pi}\cos^2\psi d\psi}{\int_0^\pi\sin\theta_P d\theta_P\int_0^{2\pi}d\varphi\int_0^{2\pi}d\psi} \tag{3}$$

  Integration leads to $\Delta A_{\perp}^0 \propto \frac{1}{15}$. By substituting $\Delta A_{\parallel}^0$ and $\Delta A_{\perp}^0$ in 1, one finds that $r^0(0) = \frac{2}{5}$ for parallel transition dipoles. We recall for completeness that $\Delta A_{\parallel}^0$ is 3 times larger than $\Delta A_{\perp}^0$ at time zero. The ratios between the signals at time zero and time infinitum (with ran-

domized molecular orientation) are $9/5$ and $3/5$ for parallel and perpendicular polarizations, respectively.

- **Case b, non-parallel $\vec{\mu}_{01}$ and $\vec{\mu}_{1n}$ transition dipoles.** Let α be the angle between $\vec{\mu}_{01}$ and $\vec{\mu}_{1n}$. Following similar arguments as in the previous case,[1] it can be shown that $\Delta A_{\parallel}^{\alpha}$ and $\Delta A_{\perp}^{\alpha}$ are ruled by Equations 4 and 5.

$$\Delta A_{\parallel}^{\alpha} \propto g_{01}(\nu_P) g_{1n}(\nu_{Pr}) \mu_{01}^2 \mu_{1n}^2 \frac{2\cos^2\alpha + 1}{15} \tag{4}$$

$$\Delta A_{\perp}^{\alpha} \propto g_{01}(\nu_P) g_{1n}(\nu_{Pr}) \mu_{01}^2 \mu_{1n}^2 \frac{2 - \cos^2\alpha}{15} \tag{5}$$

Accordingly, the time zero anisotropy $r^{\alpha}(0)$ depends on the angle α between the ground- and excited-state transition dipoles, Equation 6.

$$r^{\alpha}(0) = \frac{2}{5} \times \frac{3\cos^2\alpha - 1}{2} \tag{6}$$

Therefore, the anisotropy reaches a maximum value of 0.4 for $\alpha = 0$ while the minimum value is -0.2 for $\alpha = \frac{\pi}{2}$. For $\alpha \approx 0.96$ (magic angle, 54.7°) the anisotropy is zero. These conclusions may be easily generalized for several overlapping ESA bands being the measured anisotropy the weighted average of the anisotropy associated to each band. Consequently, the limiting anisotropy values remain -0.2 and 0.4 for pure ESA signals even if they arise from several independent optical transitions.

As in the previous case, we recall that the ratios between the time zero and time infinitum signals are $\frac{3(2\cos^2\alpha+1)}{5}$ and $\frac{3(2-\cos^2\alpha)}{5}$ for parallel and perpendicular polarizations, respectively. The signal ratio between parallel and perpendicular polarizations amounts to $\frac{2\cos^2\alpha+1}{2-\cos^2\alpha}$ at time zero.

- **Overlapping excited-state absorption (ESA) and stimulated emission (SE) bands with non-parallel transition dipoles.** In the following discussion, ΔA^{ESA} and ΔA^{SE} refer to transient absorption contributions associated to single ESA and SE bands. μ_{ESA} and μ_{SE} are the strengths of their transition dipoles, $g_{ESA}(\nu)$ and $g_{SE}(\nu)$ are the associated lineshape functions, while α_{ESA} and α_{SE} are the angles subtended by the ground- and the excited-state ESA and SE transition dipoles, respectively. With these definitions, the transient absorption signals measured with parallel and perpendicular pump-probe polarizations are given by Equations 7 and 8.

$$\Delta A_{\parallel}^{\alpha_{ESA},\alpha_{SE}} = \Delta A_{\parallel}^{\alpha_{ESA}} + \Delta A_{\parallel}^{\alpha_{SE}} \tag{7}$$

$$\Delta A_{\perp}^{\alpha_{ESA},\alpha_{SE}} = \Delta A_{\perp}^{\alpha_{ESA}} + \Delta A_{\perp}^{\alpha_{SE}} \tag{8}$$

The terms in Equations 7 and 8 are evaluated as in 4and 5 but the SE (the gain) enters with negative sign. Thus, the parallel and perpendicular transient absorption signals are governed by Equations 9 and 10, respectively.

$$\Delta A_{\parallel} \propto \frac{g_{01}(\nu_P)\mu_{01}^2}{15}\left[g_{ESA}(\nu_{Pr})\mu_{ESA}^2(2\cos^2\alpha_{ESA}+1) - g_{SE}(\nu_{Pr})\mu_{SE}^2(2\cos^2\alpha_{SE}+1)\right] \tag{9}$$

$$\Delta A_{\perp} \propto \frac{g_{01}(\nu_P)\mu_{01}^2}{15}\left[g_{ESA}(\nu_{Pr})\mu_{ESA}^2(2-\cos^2\alpha_{ESA}) - g_{SE}(\nu_{Pr})\mu_{SE}^2(2-\cos^2\alpha_{SE})\right] \tag{10}$$

The measurements done at each polarization enter the definition in 1 to yield the anisotropy in the spectral region where ESA and SE overlap, 11.

$$r_{\alpha_{ESA},\alpha_{SE}}(0) = \frac{g_{SE}(\nu_{Pr})\mu_{SE}^2\left[1-3\cos^2\alpha_{SE}\right] - g_{ESA}(\nu_{Pr})\mu_{ESA}^2\left[1-3\cos^2\alpha_{SE}\right]}{5\left[g_{ESA}(\nu_{Pr})\mu_{ESA}^2 - g_{SE}(\nu_{Pr})\mu_{SE}^2\right]} \tag{11}$$

Note that the anisotropy may take values beyond -0.2 and 0.4 when ESA and SE bands overlap. This behavior becomes evident when both bands show similar strength and the denominator approaches zero, *i.e.* in the neighborhood of isosobestic points. Characteristic dispersive features are observed at these positions in the anisotropy spectrum.[2] To put an example, assume that $g_{ESA}(\nu_{Pr})\mu^2_{ESA} = 3/2 \times g_{SE}(\nu_{Pr})\mu^2_{SE}$ and the angles for the transition dipoles are $\alpha_{ESA} = \pi/2$ and $\alpha_{SE} = \pi/4$; the resulting anisotropy is $r(0) = -0.44$. The same holds for overlapping ESA and bleach regions.

Basis set for spectral decomposition

The basis spectra employed in the spectral decomposition of transient absorption data of cryptochrome are shown, Figures S1-S3. A brief account of the methods employed to estimate the spectral shapes and molar extinction coefficients is given.

The excited-state (S_1) spectrum of FAD was calculated from transient and ground state absorption spectra of riboflavin in neutral water.[2,3] Several spectral features of riboflavin suggest that neutral water is a reasonable model of the protein pocket in cryptochrome. First, the $S_2 \leftarrow S_0$ absorption band is centered at 360 nm in water at neutral pH while in acetonitrile, ethanol and dimethyl sulfoxide the band peaks at 354, 350 and 345 nm, respectively.[2] Second, the ratio between the stimulated emission and the $S_0 \rightarrow S_1$ bleach bands is less than one in water but practically one in other polar solvents.[2] In the case of CPH1, the second absorption band is centered around 368 nm[4] and the ratio of SE to bleach bands in the early transient spectra is clearly less than one (see Figure 1). Finally, the shoulder in ESA at about 400 nm is characteristic of early transient absorption in water and it is also prominent in the transient spectra of CPH1. In all other polar solvents studied this feature is not found. These observations suggest that neutral water resembles the solute-solvent interactions experienced by flavin in the protein pocket.

The transient spectrum of the S_1 state was obtained by assuming first that excited state absorption is negligible at 450 nm. Normalization and subtraction of the ground-state absorption

spectrum of riboflavin from the transient absorption at 2 ps yielded the bleach-free linear absorption spectrum of S_1 (spectral relaxation is over at 2 ps delay in water) (Figure 1). Alternatively, transient and ground-state absorption spectra may be decomposed as a sum of *log-normal* functions accounting for independent optical transitions starting from the S_1 and S_0 electronic states, respectively. The $S_0 \rightarrow S_1$ bands obtained in this way for ground-state absorption and S_1 transient absorption (where $S_0 \rightarrow S_1$ contributes as bleach, with negative sign) are nearly indistinguishable. Only $S_1 \rightarrow S_n$ transitions remain after normalization of the individual $S_0 \rightarrow S_1$ bands and subtraction (green line in 1). Both approaches lead to essentially the same bleach-subtracted spectrum of the S_1 state corroborating that S_1 ESA is indeed negligibly small at 450 nm. This is consistent with a constant value of ≈ 0.4 for the anisotropy at 450 nm.

Parallel transient spectra of CPH1-PHR were analyzed rather than magic-angle because of the better signal/noise ratio. Consistently, transient spectra of S_1 measured with parallel polarization were used. Yet, one faces a different situation with basis spectra obtained from isotropically-distributed samples, such as those of Trp radicals and FAD anion radical. The relative amplitudes of the bands will in general differ from those observed after photoselection with the pump laser. This was taken into account. We first observed that the anisotropy at 370 nm does not evolve in time despite the charge transfer reaction. Taken together with the spectral decomposition in Figure 6, it is deduced that a) the FAD transition dipoles μ_{01} and μ_{1n} are oriented at an angle of $\approx 25^{\circ}$ and b) FAD μ_{1n} and $FAD^{\cdot -}$ μ_{0n}, both with maxima at $\approx$ 370 nm, are approximately parallel. It results that the optical spectrum of the isotropically distributed FAD anion radical is close to the parallel spectrum. Second, the relative amplitudes of the visible and UV bands of the Trp radicals in the transient spectrum could vary from those observed in the isotropic sample and used in the basis set. However, this effect is expected to be minor because the transient absorption in the UV is dominated by S_1 FAD and FAD anion radical. The reasonable magnitude of the transient concentrations obtained from the spectral analysis supports our choice of basis spectra.

The difference spectrum of the flavin anion radical of CPH1-PHR was determined in the D393C

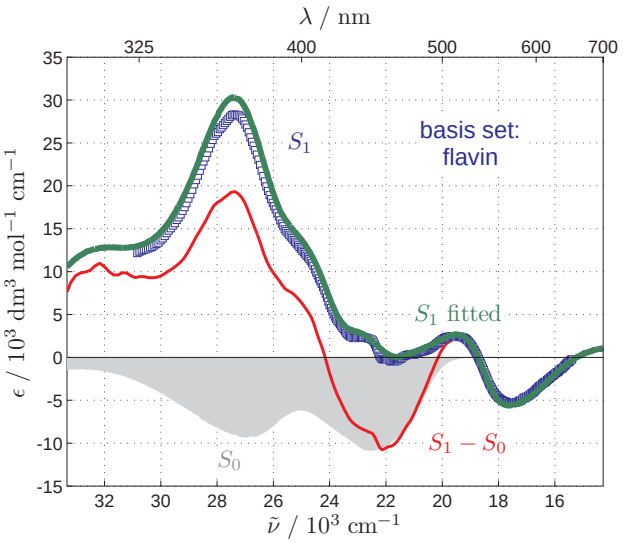

Figure S 1: Estimation of the molar absorption coefficient of the oxidized flavin in the S_1 state. The spectrum of the S_1 state (blue) was obtained by normalization and subtraction of the transient absorption spectrum of riboflavin measured at long delay times in water (red) and the steady-state absorption spectrum of riboflavin (gray). Alternatively, the S_1 spectrum may be obtained by spectral decomposition with log-normal functions and normalization (green), see text. Both methods produce nearly indistinguishable spectra.

mutant after blue light illumination (A. Hense and T. Kottke, unpublished results). Compared to anion radical spectra from *Drosophila* cryptochrome, glucose oxidase or free flavin, significant differences in terms of band position, relative band strength and sharpness of vibrational structure were observed.[5,6] We found that these differences influence the outcome of the fit, *i.e.* it is quite important to preserve the environment of the anion radical. For the flavin neutral radical the difference spectrum was measured in wild-type CPH1-PHR, where the neutral radical forms in microseconds.[4] The molar extinction coefficients of FAD anion and neutral radical were estimated from pulse radiolysis spectra published by Land and Swallow.[7]

Spectra of tryptophan cation and neutral radicals were calculated by digitization and fit with *log-normal* functions of spectra of Solar *et al.* in water.[8]

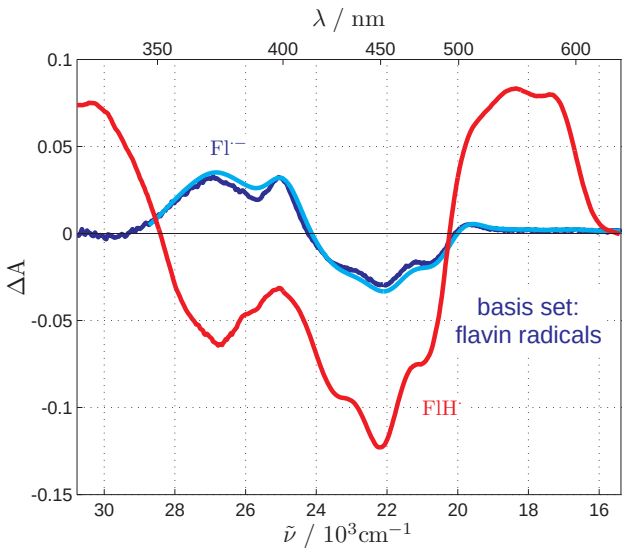

Figure S 2: Difference UV–vis absorption spectra (radical – oxidized) measured for the flavin (Fl) chromophore in the protein environment. The spectrum of the neutral radical ($FlH^{\cdot}$) is shown in red while that of the anion radical ($Fl^{\cdot -}$) is shown in blue. The latter was convoluted with a 10 nm gaussian function to account for the spectral resolution of the femtosecond experiment (cyan).

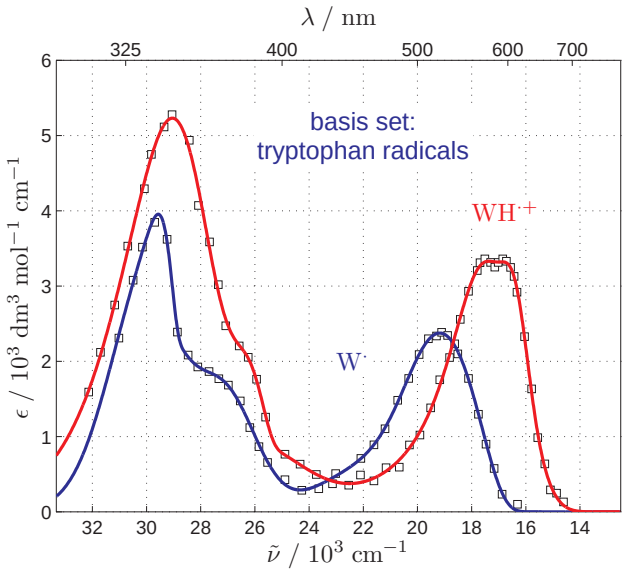

Figure S 3: UV–vis absorption spectra of tryptophan cation radical (red) and tryptophan neutral radical (blue). The spectra were scanned from the work of Solar *et al.* (Figure 1 of *J. Phys. Chem.* **1991**, *95*, 3639-3643), digitalized (squares) and fitted to a set of log-normal functions (lines).

Cooling timescale and global fits of band integrals.

Vibrational cooling in the protein environment has been observed with different kinds of fs spectroscopy and studied by computer simulations. Among others, heme proteins [9,10] (hemoglobin,[9,11,12] myoglobin,[9,13] cytochrome *c*[14–16]), bacteriorhodopsin,[17,18] channelrhodopsin-2,[19] green fluorescent protein,[20] plastocyanines,[21] phytochromes[22,23] and flavoproteins[24] have been addressed by many groups. Remarkably, this effect was not considered in fs and early ps studies of cryptochromes and photolyases. There is ample consensus about the main component of vibrational cooling in proteins. It ranges from 2[18,21] to 10 ps.[20] While extraction of cooling time-constants from ultrafast experiments is not straightforward, this view was corroborated by computer simulations by the Straub's group.[25–28] They indicate that the molecular temperature decays exponentially with sub-10 ps time-constants both in cytochrome *c*, where chromophore to protein energy transfer is supposed to occur,[28] and in myoglobin, where energy is conducted directly from the heme group to the solvent.[27]

However, some ultrafast Raman[13] and IR[9] measurements provided direct evidence of bimodal vibrational cooling with time constants in the range of 2-9 and $\approx$ 15-25 ps. 15-25 ps constants are consistent with heat diffusion from the chromophore through the protein to the surrounding solvent.[9] Unlike most of the approaches, these two experiments were specifically designed to monitor the molecular temperature through the anti-Stokes to Stokes band ratio[13] or via the increase of D_2O transmission in the 1800 cm^{-1} region.[9] Computer simulations by Henry *et al.*[29] provide further support: 1-4 ps (50%) and 20-40 ps.

Tables S1 to S3 summarize the results of multiexponential fits to band integrals. Approximate isosbestic points were used to define the bands. Thus, Band I is calculated from 300 to 414 nm; Band II from 486 to 540 nm; Band III from 540 to 585 nm and Band IV from 585 to 670 nm. Measurements done with 0.2 and 2 ps steps with parallel and magic angle polarization were analyzed both globally (Tables 1 and 2) and independently (Table 3). Bi- and tri-exponential functions were employed. Four decay times were identified. The four decay times are essentially the same for parallel, perpendicular and magic angle polarizations, which indicates that rotational diffusion plays no role in the sub-ns window.[30] $\tau_1 < 1$ ps accounts for the primary electron-transfer process. It is determined with high accuracy in the central region of the spectral window for low scan rates, *i.e.* 2-200 fs steps. Time accuracy deteriorates in the wings because of group velocity dispersion. The effect is also noticeable in global analyses across the full spectral window. We propose that τ_2 and τ_3 monitor vibrational cooling. For example, a global fit of band integrals for 2 ps measurements with parallel polarization yields $\tau_2 = 4 \pm 1$ and $\tau_3 = 29 \pm 7$ ps. τ_4 is determined with very poor accuracy, could range from 0.3 to 1.5 ns and may reflect radical pair recombination.

To summarize, the 31 ps time constant might indicate diffusional energy flow from the pocket, through the protein, to the solvent shell.

Table S 1: Global analysis of band integrals calculated for measurements done with 0.2 and 2 ps step size.

Fit Description	Range	τ_1 ps	τ_2 ps	τ_3 ps	τ_4 ps
$\parallel$	Band I	0.24 ± 0.04	9.7 ± 0.9		280 ± 30
	Band II	0.16 ± 0.03	13 ± 5		
	Band III	0.6 ± 0.1	10 ± 1		
	Band IV	0.7 ± 0.2		40 ± 20	
magic angle	Band I	0.1 ± 0.04	9.4 ± 0.8		230 ± 20
	Band II	0.2 ± 0.5		29 ± 3	
	Band III	0.6 ± 0.1	18 ± 5		410 ± 110
	Band IV	0.6 ± 0.3	14 ± 2		400 ± 170

Table S 2: Global analysis of all band integrals calculated for either 0.2 or 2 ps measurements with parallel or perpendicular polarization.

Fit Description	Range	τ_1 ps	τ_2 ps	τ_3 ps	τ_4 ps
0.2 ps, $\parallel$	all bands	0.14 ± 0.01	6.0 ± 0.4		
0.2 ps, magic angle	all bands	0.30 ± 0.01	16 ± 1		
2 ps, $\parallel$	all bands		4 ± 1	29 ± 7	1000 ± 700
2 ps, magic angle	all bands		10 ± 2	50 ± 30	420 ± 70

Table S 3: Free fits of band integrals

Fit Description	Range	τ_1 ps	τ_2 ps	τ_3 ps	τ_4 ps
0.2 ps, $\parallel$	Band I	0.10 ± 0.01	14.7 ± 0.7		
		0.07 ± 0.01	2.9 ± 0.4	29 ± 3	
	Band II	0.1 ± 0.1		20 ± 5	
	Band III	0.4 ± 0.04	10 ± 1		
	Band IV	0.5 ± 0.2		50 ± 70	
2 ps, $\parallel$	Band I		15 ± 1		460 ± 40
			12 ± 2	80 ± 70	760 ± 510
	Band II				
	Band III		11 ± 12	90 ± 200	1000 ± 3000
	Band IV		2 ± 3	50 ± 50	
0.2 ps, magic angle	Band I	0.08 ± 0.01	16 ± 1		
		0.05 ± 0.01	6 ± 1	40 ± 10	
	Band II	0.1 ± 0.1		19 ± 2	
	Band III	0.40 ± 0.04	7 ± 2		
	Band IV	0.3 ± 0.2		21 ± 3	
		0.6 ± 0.3	5 ± 3	120 ± 200	
2 ps, magic angle	Band I			15 ± 2	510 ± 70
			11 ± 4	40 ± 50	650 ± 240
	Band II			16 ± 3	520 ± 130
	Band III		12 ± 3		400 ± 100
			8 ± 6	50 ± 100	300 ± 200
	Band IV		12 ± 5		240 ± 60

Notes and References

(1) The solution is straightforward if Euler angles are used to define the orientation of the transition dipoles relative to the coordinate system of the laboratory.

(2) Weigel, A.; Dobryakov, A. L.; Veiga, M.; Lustres, J. L. P. *J. Phys. Chem. A* **2008**, *112*, 12054–12065.

(3) Weigel, A.; Dobryakov, A.; Klaumuenzer, B.; Sajadi, M.; Saalfrank, P.; Ernsting, N. P. *J. Phys. Chem. B* **2011**, *115*, 3656–3680.

(4) Immeln, D.; Schlesinger, R.; Heberle, J.; Kottke, T. *J. Biol. Chem.* **2007**, *282*, 21720–21728.

(5) Hanine-Lmoumene, C. E.; Lindqvist, L. *Photochem. Photobiol.* **1997**, *66*, 591–595.

(6) Berndt, A.; Kottke, T.; Breitkreuz, H.; Dvorsky, R.; Hennig, S.; Alexander, M.; Wolf, E. *J. Biol. Chem.* **2007**, *282*, 13011–13021.

(7) Land, E. J.; Swallow, A. J. *Biochem.* **1969**, *8*, 2117–2125.

(8) Solar, S.; Getoff, N.; Surdhar, P. S.; Armstrong, D. A.; Singh, A. *J. Phys. Chem.* **1991**, *95*, 3639–3643.

(9) Lian, T.; Locke, B.; Kholodenko, Y.; Hochstrasser, R. *J. Phys. Chem.* **1994**, *98*, 11648–11656.

(10) Kruglik, S. G.; Lambry, J.-C.; Martin, J.-L.; Vos, M. H.; Negrerie, M. *J. Raman Spectrosc.* **2011**, *42*, 265–275.

(11) Petrich, J. W.; Martin, J. L.; Houde, D.; Poyart, C.; Orszag, A. *Biochemistry* **1987**, *26*, 7914–7923.

(12) Lingle, R.; Xu, X. B.; Zhu, H. P.; Yu, S. C.; Hopkins, J. B. *J. Phys. Chem.* **1991**, *95*, 9320–9331.

(13) Mizutani, Y.; Kitagawa, T. *Science* **1997**, *278*, 443–446.

(14) Negrerie, M.; Cianetti, S.; Vos, M. H.; Martin, J. L.; Kruglik, S. G. *J. Phys. Chem. B* **2006**, *110*, 12766–12781.

(15) Loewenich, D.; Kleinermanns, K.; Karunakaran, V.; Kovalenko, S. A. *Photochem. Photobiol.* **2008**, *84*, 193–201.

(16) Zang, C.; Stevens, J. A.; Link, J. J.; Guo, L.; Wang, L.; Zhong, D. *J. Am. Chem. Soc.* **2009**, *131*, 2846–2852.

(17) Doig, S. J.; Reid, P. J.; Mathies, R. A. *J. Phys. Chem.* **1991**, *95*, 6372–6379.

(18) Diller, R.; Maiti, S.; Walker, G. C.; Cowen, B. R.; Pippenger, R.; Bogomolni, R. A.; Hochstrasser, R. M. *Chem. Phys. Lett.* **1995**, *241*, 109–115.

(19) Verhoefen, M.-K.; Bamann, C.; Bloecher, R.; Foerster, U.; Bamberg, E.; Wachtveitl, J. *Chemphyschem* **2010**, *11*, 3113–3122.

(20) Stoner-Ma, D.; Jaye, A. A.; Ronayne, K. L.; Nappa, J.; Meech, S. R.; Tonge, P. J. *J. Am. Chem. Soc.* **2008**, *130*, 1227–1235.

(21) Nagasawa, Y.; Fujita, K.; Katayama, T.; Ishibashi, Y.; Miyasaka, H.; Takabe, T.; Nagao, S.; Hirota, S. *Phys. Chem. Chem. Phys.* **2010**, *12*, 6067–6075.

(22) van Thor, J. J.; Ronayne, K. L.; Towrie, M. *J. Am. Chem. Soc.* **2007**, *129*, 126–132.

(23) Schumann, C.; Gross, R.; Wolf, M. M. N.; Diller, R.; Michael, N.; Lamparter, T. *Biophys. J.* **2008**, *94*, 3189–3197.

(24) Gauden, M.; Yeremenko, S.; Laan, W.; van Stokkum, I. H. M.; Ihalainen, J. A.; van Grondelle, R.; Hellingwerf, K. J.; Kennis, J. T. M. *Biochemistry* **2005**, *44*, 3653–3662.

(25) Xu, D.; Martin, C.; Schulten, K. *Biophys. J.* **1996**, *70*, 453–460.

(26) Bu, L. T.; Straub, J. E. *J. Phys. Chem. B* **2003**, *107*, 10634–10639.

(27) Zhang, Y.; Fujisaki, H.; Straub, J. E. *J. Phys. Chem. B* **2007**, *111*, 3243–3250.

(28) Zhang, Y.; Straub, J. E. *J. Phys. Chem. B* **2009**, *113*, 825–830.

(29) Henry, E. R.; Eaton, W. A.; Hochstrasser, R. M. *Proc. Natl. Acad. Sci. U. S. A.* **1986**, *83*, 8982–8986.

(30) Brazard, J.; Usman, A.; Lacombat, F.; Ley, C.; Martin, M. M.; Plaza, P.; Mony, L.; Heijde, M.; Zabulon, G.; Bowler, C. *J. Am. Chem. Soc.* **2010**, *132*, 4935–4945.